AIAA 81-1434R

Flowfield Analysis of a Scramjet Combustor with a Coaxial Fuel Jet

J. A. Schetz,* F. S. Billig,† and S. Favin‡
Applied Physics Laboratory, The Johns Hopkins University, Laurel, Md.

A calculation procedure for predicting turbulent mixing and burning and skin friction and wall heat transfer in a scramjet combustor with a central fuel jet from a gas generator has been developed. All the important physical and chemical processes have been modeled, including the upstream influence of heat release on the initial conditions and the pressure distribution in the duct. Calculations for a representative engine with Shelldyne H fuel at Mach 4 and 7 indicate that a combustor 1 to 2 m long is sufficient to insure complete heat release but that substantial nonuniformity of the combustor exit flow would still exist. The skin friction and wall heat transfer are both shown to be very sensitive to the local pressure gradient and to the impingement of combustion products and turbulence from the central jet mixing and burning zone. However, the responses of these two quantities are not of the same importance, and they are not in phase.

Nomenclature

a_2 = constant in turbulence model
$A(x)$ = duct area
A_i, B_i = constant in specific heat representation for species i
$b(x)$ = mixing zone width
C_f = skin friction coefficient
C_D = constant in turbulence model
C_2 = constant in turbulence model, ℓ/b
c_{P_i} = specific heat of species i
D_j = initial diameter of the jet
D_{ij} = binary laminar diffusion coefficient
D_T = turbulent diffusion coefficient
h = static enthalpy
H = stagnation enthalpy
k = turbulent kinetic energy (TKE)
ℓ = mixing length
Le_i = laminar Lewis number for species i
Le_T = turbulent Lewis number
M = Mach number
P = pressure
P_s = matched pressure in shock expansion zone
Pr = laminar Prandtl number
Pr_k = Prandtl number for TKE
Pr_T = turbulent Prandtl number
$\dot{q}_w$ = wall heat transfer rate
r = radial coordinate
S_0 = length of upstream portion of separated zone
T = temperature
T_r = reference temperature
u = axial velocity
u_* = friction velocity, $\equiv\sqrt{\tau_w/\rho}$
W_i = molecular weight of species i
x = axial coordinate
y = normal coordinate in the wall boundary layer
Y_i = molecular mass fraction of species i
Ψ = axisymmetric streamfunction
ρ = density
μ = laminar viscosity
μ_T = turbulent viscosity
ϵ = exponent in pressure/area relation
ν = laminar kinematic viscosity
τ_T = turbulent shear stress
Δ_i = enthalpy of species i at the reference temperature
δ^* = displacement thickness

Subscripts

c = conditions on centerline
e = conditions at the outer edge of the wall boundary layer
j = conditions in jet
0 = conditions in freestream
w = conditions on the wall

Presented as Paper 81-1434 at the AIAA/SAE/ASME 17th Joint Propulsion Conference, Colorado Springs, Colo., July 27-29, 1981; submitted Aug. 6, 1981; revision received Feb. 4, 1982. Copyright © American Institute of Aeronautics and Astronautics, Inc., 1981. All rights reserved.

*Consultant, also Professor and Chairman, Aerospace and Ocean Engineering Dept., Virginia Polytechnic Institute and State University. Associate Fellow AIAA.
†Assistant Supervisor, Aeronautics Division. Fellow AIAA.
‡Senior Programmer.

Introduction

ANALYTICAL prediction of the flowfield in the combustion chamber of a scramjet or any airbreathing engine is important to assure that sufficient length for efficient heat release has been provided over the range of expected operating conditions, to determine the distribution of heat transfer and skin friction, and to define the degree of nonuniformity of the flow leaving the combustor, so that the flow in the nozzle and in turn the exit thrust can be determined. Heat transfer predictions are important for designing engine cooling systems and structure; skin friction values are important for calculating overall system performance. In general, these flowfields are quite complex. Currently our capability to carry out reasonably detailed analysis is restricted to but a few injector/combustor geometries. An analysis of the flowfield in the supersonic combustor of the engine shown in Fig. 1 from Ref. 1 was deemed to be within the reach of current models and methods. This paper describes the development of such an analysis.

Figure 1a shows the boost phase configuration of a new propulsion concept, the integral rocket-dual combustion ramjet. During the boost phase, the combustion chambers are filled with a solid propellant, the incoming air ducts are blocked with frangible port covers, and the external compression surfaces are covered by a low drag shroud. When the rocket propellant is consumed, the exit nozzles, frangible port

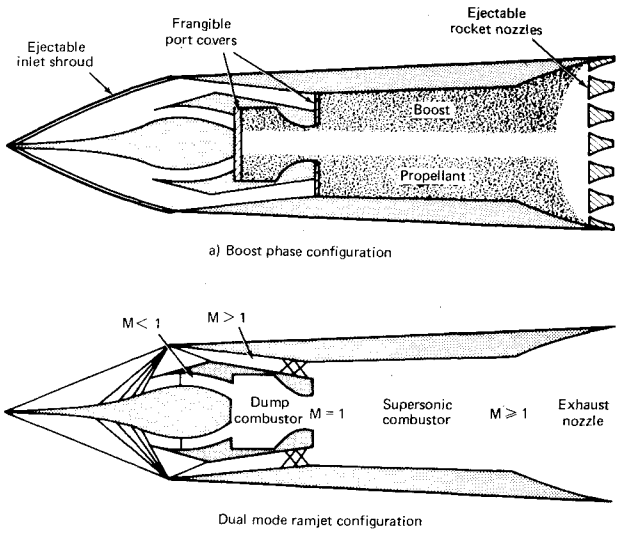

Fig. 1 Schematic illustration of integral rocket dual combustion ramjet.

covers, and the inlet shroud are ejected, air enters the inlet and the engine functions as a dual-combustion ramjet as shown in Fig. 1b. The externally compressed air is subdivided by the inner cowl lip such that a small fraction is ducted to a small, subsonic combustor. All the fuel is added in the subsonic combustor, which acts as a fuel-rich, hot-gas generator for the supersonic combustor. The major portion of the air bypasses the gas generator and is ducted through an air conduit to the supersonic combustor, where it mixes and burns with the exhaust of the gas generator. The final shocks shown in the supersonic duct result from the combustion-induced pressure disturbances generated by the mixing and heat release processes.

A modular approach to the analysis of this complex flowfield was adopted. The mixing and burning of the center jet was treated with one computer code, and a separate wall boundary-layer calculation procedure was then coupled to it. This approach is suggested mainly by the substantial difference in grid resolution required in these two parts of the flow. A much finer grid is required in the boundary layer than in the mixing and burning zone, so that wall properties can be predicted accurately.

The main mixing and burning calculation is made with an extended version of the code presented in Ref. 2. The initial building blocks for that work were the nonreacting, turbulent jet mixing code of Ref. 3; the integrated, turbulent kinetic energy (TKE) method for calculating the eddy viscosity from Ref. 4; the double flame-sheet model of Ref. 5; the chemical equilibrium calculation procedure of Ref. 6; and the integral, confined flow with heat release treatment of Refs. 1 and 7.

Most of the required modifications were incorporated into a greatly extended version of the mixing code of Ref. 3. The first extension was to accommodate confined mixing in a duct with a central fuel jet rather than jet mixing in an infinite stream. This was accomplished by holding the stream function along the outer boundary fixed at its initial value in order to maintain a constant total mass flow in the duct. Velocity "slip" was allowed along the duct wall. Two options are incorporated: in the first, $P(x)$ is specified and $A(x)$ is computed; in the second, the inverse is done. The second extension undertaken was to incorporate a more advanced turbulent transport model.

The third and largest extension made was to incorporate equilibrium chemical reactions into the mixing zone. The chemical system is written to include H, C, O, and N atoms in the following molecular combinations: O_2, N_2, H_2, CO, CO_2, H_2O, OH, O, H, N, and NO. Because of the high static pressures and temperatures, and the great simplicity thereby introduced, local, diffusion-controlled, chemical equilibrium was assumed to apply. The computer code given in Ref. 6 was modified extensively to enable more efficient calculations. This results in a reduction in the cost per calculation for an enthalpy-pressure (h, P) entry from \$0.1-0.5 to about \$0.01 per point. It was still necessary to introduce further simplifications to bring the computation cost to an acceptable level. To exemplify this point, consider the following typical case. For a 2-m long, 0.1-m radius duct, about 25 radial points and 1000 axial stations are required to obtain acceptably accurate solutions; at \$0.01 per point the cost of the equilibrium calculations is about \$250-\$500 as compared with a cost of less than \$50 for the mixing calculations and all other input and output. Clearly, some rational approximation to decrease the number of required equilibrium calculations is in order. Thus, the double flame-sheet model of Ref. 5 was adapted to the present problem. Simply stated, the model considers an inner H_2 flame and an outer CO flame with only the O_2, H_2, N_2, H_2O, CO, and CO_2 molecular species assumed to be present. As long as the temperature remains below about 2500 K, the model provides a good approximation to the exact equilibrium state. Therefore, a composite model was adopted. At each axial station, a complete calculation is made using the double flame-sheet model. The temperature profile is searched for points having a predicted temperature greater than 2500 K. For those points a complete equilibrium calculation is made before moving to the next axial station. The resulting cost reduction factor has been about three to five.

One important point remained. The mixing and burning code itself is based on the boundary-layer form of the equations of motion; hence, the formulation is parabolic, and no upstream influence is possible. On the other hand, it is well known that heat release in a duct affects the initial conditions, even for supersonic flow.[7] This critical behavior was included by using the integral analysis of Refs. 1 and 7 to set the initial conditions and $P(x)$ along the duct.

For our purposes here, it was necessary to extend the method of Ref. 2 one step further. One can anticipate that the impingement of the hot combustion products from the main mixing and burning region on the outer edge of the wall boundary layer will significantly influence wall heat transfer and skin friction. In addition, however, the turbulence produced in that shear layer will also impinge on the wall boundary layer, and that can also be expected to influence the boundary layer. The effect will be similar to that for a boundary layer with high freestream turbulence. We, therefore, require a prediction of the turbulence level at the edge of the mixing and burning shear layer to be used as outer boundary conditions for the wall boundary-layer computation. The integrated TKE model used in Ref. 2 is based on average values of the TKE across the mixing zone, and the detailed profiles are not predicted. Therefore, we have now modified the code to include the solution of a partial-differential equation for the detailed distribution of the TKE. The modeling follows the Prandtl energy method.[8]

For the combustor wall boundary-layer part of the flowfield calculations, we again sought to adopt or adapt existing codes where possible. There are a number of elaborate computer codes available for the calculation of boundary-layer flows under turbulent, high-speed flow conditions (e.g., Refs. 9 and 10). A comprehensive review of the subject of the numerical calculation of reacting, laminar boundary layers may be found in Ref. 11. None of these codes is, however, suitable for calculating the boundary layer on the walls of a scramjet combustor. The major shortcomings are that the chemistry generally is limited to air and not fuel-air mixtures and provisions for the entrainment of rapidly streamwise varying, boundary-layer "edge" conditions under turbulent conditions have not been made. In the present case, this occurs due to the impingement of the edge of the jet mixing zone on the wall boundary layer. The extension to

include reactive mixtures of the H-C-O-N system involves not only chemistry but significant complications in terms of the laminar physical properties such as viscosity, Prandtl number, and Lewis number of the resulting mixtures. There are also important new questions with regard to the modeling of turbulent transport processes in these types of flows. The basic finite-difference methods of Ref. 9 were selected for the numerical solution of the equations of motion. The physical properties procedures were taken from Ref. 12.

The boundary-layer flows of interest differ from those usually encountered in at least two important ways. First, we have the diffusion of products of combustion in from the outer edge. This changes the distribution of density and physical properties (among other things) across the whole layer. Second, the rapidly varying boundary-layer edge conditions result in profiles of unusual shape in the outer part of the layer. Under these circumstances, one is reluctant to simply apply turbulent transport models that have been developed and tested only for conventional boundary-layer flows. This is all the more true since those models cannot respond directly to the types of new effects mentioned earlier. Thus, one is led to seek a model at a higher (and more fundamental) level than a mean-flow type, such as an algebraic eddy viscosity or mixing length model. The next level of model is based on the variation of the kinetic energy of turbulent fluctuations,

$$k \equiv \frac{\overline{u^2+v^2+w^2}}{2} \tag{1}$$

in the flow. Prandtl[8] suggested the form of one such approach. A turbulent viscosity μ_T is related directly to k with a length scale ℓ as

$$\mu_T = \rho\sqrt{k}\ell \tag{2a}$$

The variation of ℓ is specified algebraically, but a separate conservation equation for k must now be solved along with the other equations of motion. Importantly, the equation for k involves terms for the production and dissipation of turbulence that depend upon the profile shape. Thus, turbulent transport is made sensitive to any new processes that influence profile shape such as those of interest in the present problem. Therefore, this model has been implemented in our wall boundary-layer code.

In the following sections, the details of the various new parts of the analysis are described, starting with the extension of the jet mixing and burning code for the Prandtl energy method. The boundary-layer analysis is then presented in detail. Both analyses are tested by comparison with relevant experiments for simpler special cases. Next, the coupling of the various modular parts of the calculation procedure is shown. Lastly, the results of some representative cases for a scramjet combustor are presented and discussed.

Analysis

Prandtl Energy Method for Jet Mixing

The Prandtl energy method[8] is based on an eddy viscosity model that is tied directly to the variation of turbulent kinetic energy, $k(x,r)$ throughout the flow by

$$\tau_T = \mu_T \frac{\partial u}{\partial r} = \rho\sqrt{k}\ell\frac{\partial u}{\partial r} \tag{2b}$$

where ℓ is the mixing length taken as a fraction C_2 of the mixing zone width $b(x)$ for free shear flows.

The variation of $k(x,r)$ is determined by the solution of an appropriately modeled conservation equation.

$$\rho u\frac{\partial k}{\partial x}+\rho v\frac{\partial k}{\partial r}=\frac{1}{r}\frac{\partial}{\partial r}\left(\frac{\mu_T r}{Pr_k}\frac{\partial k}{\partial r}\right)+\mu_T\left(\frac{\partial u}{\partial r}\right)^2-\frac{C_D\rho k^{3/2}}{\ell} \tag{3}$$

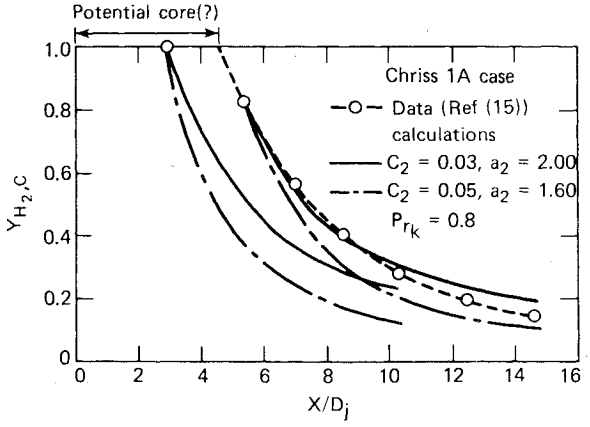

Fig. 2 Comparison of predictions with the TKE model and the experiments of Ref. 9; centerline concentration.

Here, Pr_k is a turbulent "Prandtl" number for k and C_D is a constant in the viscous dissipation of turbulence term. This is often expressed in terms of another constant a_2 related to C_D as

$$C_D/\ell = a_2/b \tag{4}$$

Some further discussion of the rationale for this type of model can be found in Ref. 13. This equation was transformed into von Mises coordinates (x,Ψ) and solved numerically by the same methods as for the momentum, energy, and species equations in Ref. 3. That work was adapted from the original work in Ref. 14.

A comparison of prediction and experiment for the case of a pure H_2 jet into air[15] is shown in Fig. 2. Due to the very large difference in molecular weights of these gases, the effects of density in this case are extreme, yet quite reasonable agreement can be noted. We have chosen $a_2 = 1.60$ and $C_2 = 0.05$ on the basis of this comparison and others. The choice was influenced by the decay rate of centerline concentration for $x/D_j \gg 1$. The turbulent Prandtl number Pr_T was taken as 0.75, the turbulent Lewis number Le_T was taken as 1.0, and the Prandtl number for TKE, Pr_k, was taken as 0.8.

Wall Boundary-Layer Calculation

We undertook substantial extensions and modifications to the code of Ref. 9 to make it applicable to the present problem. First, species conservation equations for the various species in terms of mass fraction Y_i were introduced

$$\rho u\frac{\partial Y_i}{\partial x}+\rho v\frac{\partial Y_i}{\partial y}=\frac{\partial}{\partial y}\left(\rho(D_{i4}+D_T)\frac{\partial Y_i}{\partial y}\right) \tag{5}$$

Since, at this point in our efforts, only overall lean mixtures have been considered, the flame(s) do not enter the wall boundary layer and we can deal directly with molecular species rather than atomic species. By the same token, there are no chemical production terms to be considered. It is common in aerospace calculations to use a binary diffusion approximation considering the fluid, usually air, to consist only of molecules and atoms. In the present case, we have molecules ranging in molecular weight from 18 for H_2O to 44 for CO_2 with O_2 at 32 and N_2 at 28 in between. For overall fuel-rich cases, H_2 at 2 would also be present. Under these circumstances, the binary diffusion approximation is not adequate. On the other hand, the multicomponent diffusion formulation is cumbersome. Studies by Fristrom at APL have shown that an excellent, heuristic approximation to the full multicomponent formulation is obtained for air combustion problems by treating each specie as a "trace" in a mixture with N_2. Certainly the mass fractions of all other species are

small compared to that for N_2. One then uses an appropriate diffusion coefficient D_{i4} for each species i where the subscript 4 denotes N_2. All of this is, of course, only important in the region near the wall where laminar processes are significant. These equations were transformed into Levy-Lees coordinates and nondimensionalized and then solved in a separate subroutine using the "solver" routine of Ref. 9.

The second step was the addition of a term to account for energy transfer by mass transfer into the energy equation.

$$\rho u\frac{\partial H}{\partial x}+\rho v\frac{\partial H}{\partial y}=\frac{\partial}{\partial y}\left\{\left(\frac{\mu}{Pr}+\frac{\mu_T}{Pr_T}\right)\frac{\partial H}{\partial y}+\left[\mu\left(1-\frac{1}{Pr}\right)+\mu_T\left(1-\frac{1}{Pr_T}\right)\right]\frac{\partial u^2/2}{\partial y}+\left(-\frac{\mu}{Pr}+\frac{\mu_T}{Pr_T}\,(Le_T-1)\right)\times\sum_i h_i\frac{\partial Y_i}{\partial y}+\sum_i\frac{\mu}{Pr}Le_i h_i\frac{\partial Y_i}{\partial y}\right\} \tag{6}$$

The last two terms in the bracket on the right-hand side are new. Again, this equation was actually solved after being transformed into Levy-Lees coordinates.

Third, the temperature/enthalpy relations for each species were taken here as

$$h_i=\Delta_i(T_r)+\int_{T_r}^{T}c_{P_i}\mathrm{d}T \tag{7a}$$

$$c_{P_i}=A_i(T_r)+B_i(T-T_r) \tag{7b}$$

the same as for the jet mixing calculation.

The fourth step was the addition of a streamlined version of the laminar transport property calculation procedure of Ref. 12 as a subroutine. This is an important and costly (in terms of computation time) step, since the laminar viscosity, for example, is not negligible compared to the turbulent viscosity for the first ten or more grid points out from the wall. These calculations for the mixtures involved here, while straightforward following classical theory, are relatively expensive. We have not found any way to avoid that cost; we have minimized it by making the laminar transport property calculations only in the region where they contribute significantly to the overall transfer processes.

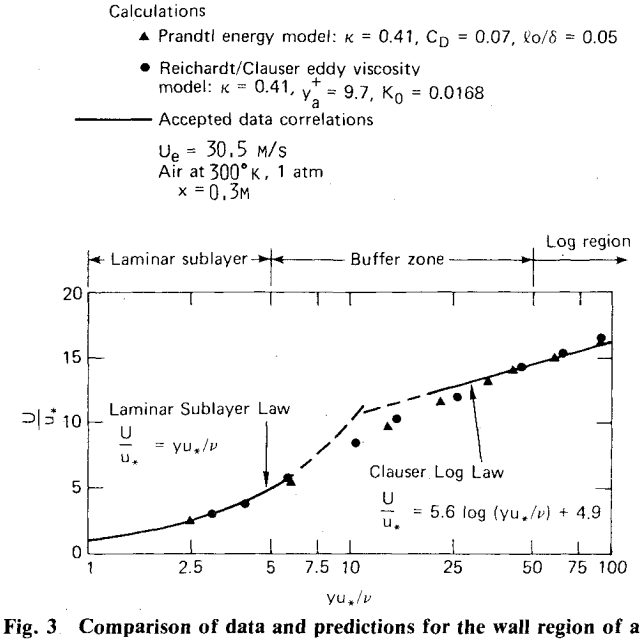

Fig. 3 Comparison of data and predictions for the wall region of a low-speed turbulent boundary layer.

The final new work undertaken was the addition of a conservation equation for the TKE suitable for the wall region

$$\rho u\frac{\partial k}{\partial x}+\rho v\frac{\partial k}{\partial y}=\frac{\partial}{\partial y}\left[\left(\frac{\mu+\mu_T}{Pr_k}\right)\frac{\partial k}{\partial y}\right]+(\mu+\mu_T)\left(\frac{\partial u}{\partial y}\right)^2-\frac{C_D\rho k^{3/2}}{\ell} \tag{8}$$

We retain

$$\mu_T=\rho\sqrt{k}\ell$$

but the relation of the length ℓ to the width of the viscous layer must be modified to account for the damping of turbulence by the wall. This length ℓ is related to the more familiar mixing length ℓ_m defined by

$$\tau_T=\rho\ell_m^2\left|\frac{\partial u}{\partial y}\right|\frac{\partial u}{\partial y} \tag{9}$$

by

$$\ell=C_D^{1/4}\ell_m \tag{10}$$

Thus, we may use Van Driest's formula for ℓ_m which accounts for wall damping[16] with Eq. (10) to give

$$\ell=C_D^{1/4}\kappa\left[1-\exp\left(\frac{\rho yu^*/\mu}{26}\right)\right] \tag{11}$$

For the outer part of the layer, we have simply

$$\ell_0=k_2\delta \tag{12}$$

All of this was put into Levy-Lees coordinates and nondimensionalized. The resulting form of Eq. (8) was solved using the solver routine of Ref. 9.

As with any turbulent transport model, there are constants that must be selected through a one-time comparison with experiment. One would also like to test the model against simple known cases in order to assess the accuracy of the predictions. For these purposes, three cases have been selected. First, low speed turbulent flow on a flat plate is considered to be known in detail.[17] The profiles near the wall take the form shown in Fig. 4 as solid lines. The result of calculations with the well-accepted Reichardt eddy viscosity distribution[18] for such cases is shown as the solid circles. The constant $\kappa=0.41$ is related to the 5.6 in the log law,[17] the $y_a^+=9.7$ in the Reichardt model[18] is related to the 4.9, and $K_0=0.0168$ comes from Ref. 17 as modified by later workers. The result of using the Prandtl energy model is shown as solid triangle symbols in Fig. 3. The Clauser skin friction law[17] gives $C_f=0.00383$ for this situation. The eddy viscosity approach gives 0.00384, and the Prandtl energy approach gives 0.00380. Clearly, good agreement with experiment and with the older eddy viscosity model results can be achieved with the Prandtl energy method and this choice of constants for this uncomplicated flow.

Here, we are concerned with high-speed flows, so a relatively simple high-speed experiment[19] has been chosen to test the prediction of our implementation of the Prandtl energy method. Of course, the values of the constants are held fixed at the values determined for the low-speed case. Some comparisons are shown in Figs. 4 and 5. At $x=54.56$ cm (21.48 in.), Coles reported a measured $C_f=0.00162$, and our Prandtl energy method gives 0.00177. We take this evidence as strong support for the utility of the Prandtl energy method, and we hope to capitalize on its more fundamental nature and greater generality for the complex boundary-layer flows in the current application.

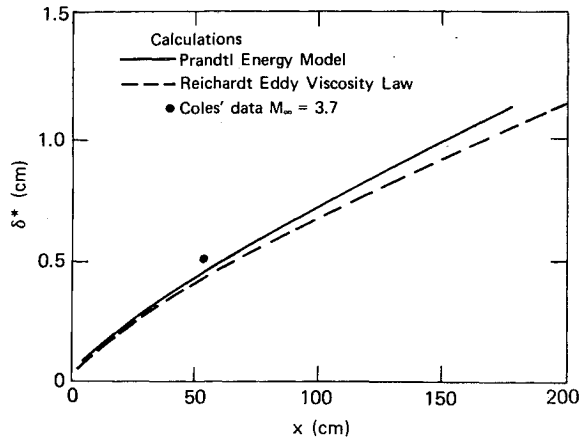

Fig. 4 Displacement thickness for Coles' flat plate data (Ref. 19).

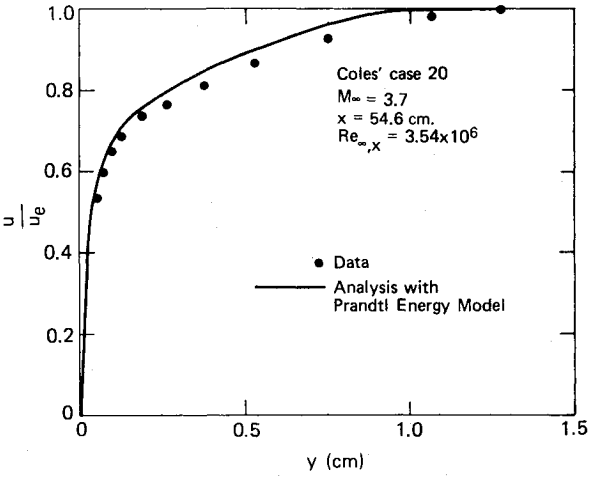

Fig. 5 Velocity profiles for Coles' flat plate data (Ref. 19).

The last test case selected involves an experimental situation[20] where the freestream turbulence level was varied over a rather wide range (approximately $0.0003 \leq k_e/u_e^2 \leq 0.009$). The influence of a high k_e on boundary-layer development is important in the present context, since the impingement of the center jet mixing zone on the wall boundary layer will involve the same processes. A comparison of predictions and experiment is shown in Fig. 6. It appears that the TKE analysis underpredicts somewhat the effects of increasing k_e, although there is considerable uncertainty in the data. Some of the discrepancy can also be traced to the fact that the experiment involved a leading-edge sand strip to trip the flow, and the analysis cannot account for that. In any event, these results can be taken as showing that the effects of varying k_e are predicted to the correct order and that the predictions are, if anything, conservative.

Numerical Examples

The various parts of the total computational scheme have been tested where possible by comparison with relevant experimental data. It was shown in Ref. 7 that the one-dimensional calculation procedure accurately predicts the upstream influence of heat release in the duct and $P(x)$. The jet mixing code was shown here to be capable of good predictions for the cases of large density variations that are of interest. Finally, the boundary-layer code was shown to be capable of predicting the effects of high external Mach numbers and high freestream turbulence levels. With that background, we are ready to make calculations for representative scramjet combustor conditions.

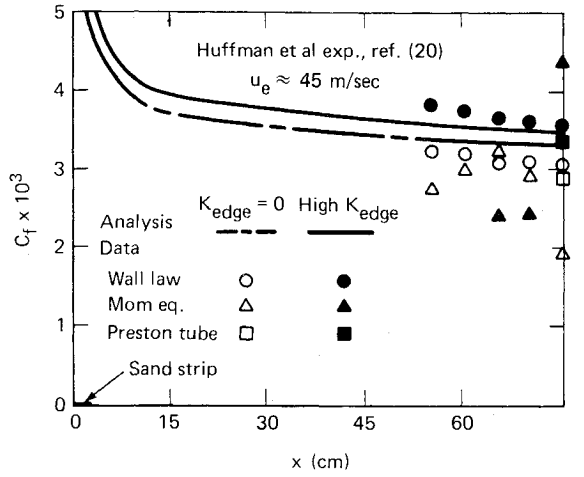

Fig. 6 Comparison of prediction and experiment for the effects of high freestream turbulence.

Detailed calculations have been made for a representative engine based on inlet design "D" from Ref. 1. Some of the pertinent features of this engine configuration are as follows:

1) The inlet compression surface is a 12.5-deg half-angle cone followed by an isentropic turn to a maximum surface angle of 27.1 deg.

2) 25% of the air captured by the inlet is ducted to the gas generator.

3) The design Mach number is 7 where the critical pressure recovery is 0.10 in the gas generator.

4) At $M_0 = 4$ the inlet air capture ratio is 0.42 and the critical pressure recovery in the gas generator is 0.46.

5) The inlet to the main combustor internally contracts the flow by 16%, giving conditions ahead of the combustor shock of $M = 2.23$ at $M_0 = 4$ and $M = 3.53$ at $M_0 = 7$.

6) The ratios of gas generator area and main combustor inlet area to engine inlet area are 0.0458 and 0.0717, respectively.

7) The combustor is a cone frustrum with an exit to inlet area ratio of 3 and a length of 1.5 m.

8) The radius of the sonic exit of the gas generator is 6.5 cm and the blunt base has a thickness of 2.5 cm.

Combustor flowfield calculations were made at flight conditions of Mach 7 at 18,500 m and Mach 4 at 11,400 m with Shelldyne H fuel at an overall equivalence ratio of 0.5.

Integral Analysis for Initial Conditions and $P(x)$

The calculations have been made with $P(x)$ and the initial conditions determined from the integral technique given in Refs. 1 and 7 from a specified combustor wall shape. This step is very important, since the system composed of the boundary-layer form of the equations of motion is parabolic. Thus, the mixing code cannot calculate the upstream influence of heat release in the duct. On the other hand, the procedure of Refs. 1 and 7 was designed to provide just that important information. A schematic representation of the flow model is depicted in Fig. 7. In the integral method, a control boundary is selected such that the flow in the entrance and exit planes can be considered one-dimensional, i.e., in the incoming air stream, in the gas generator at the sonic point, and in the combustor exit. Three major regions of the flow are defined. A shock-expansion zone is followed by a highly nonuniform combustion zone which blends into a combustion zone that is nearly one dimensional at a given flow station. In the shock-expansion zone, the flow from the gas generator and the supersonic air inlet adjust to a matched pressure P_s condition and create a separated zone on the bluff base.

In the absence of any contradictory experimental data, the average pressure on the base is assumed to be P_s. The compression field in the air stream also causes local separation on

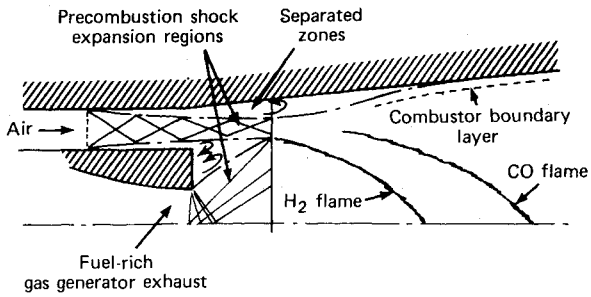

Fig. 7 Schematic illustration of the model used in the composite analysis.

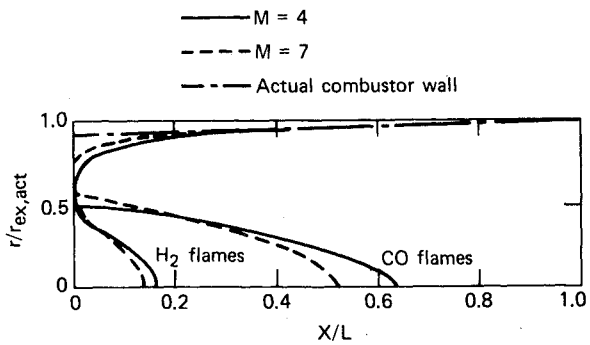

Fig. 8 Predicted duct contours and flame shapes for engine with inlet D at Mach 4 and 7 with ER = 0.5.

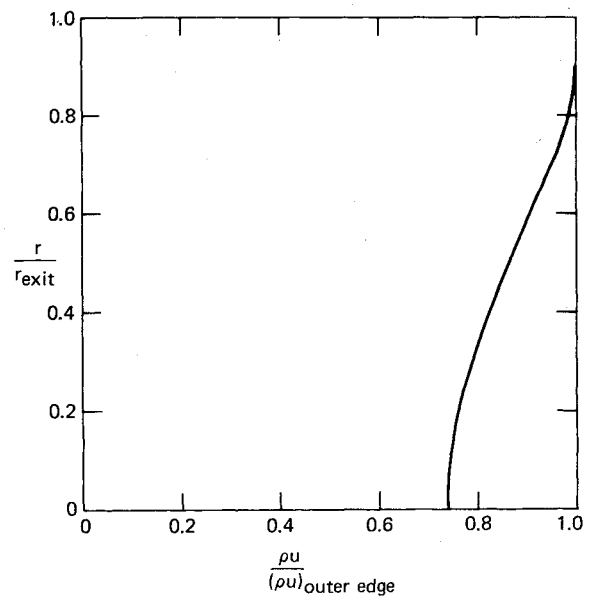

Fig. 9 Predicted combustor exit mass flux profile at Mach 7 with ER = 0.5.

the outer combustor wall that extends a distance S_0 upstream of the discharge plane of the gas generator. This distance, as well as the downstream extent of the separation zone and the wall pressure distribution therein, have been determined for conventional supersonic combustors[21] but have not been obtained in this engine configuration. Until this information becomes available, the pressure distribution used in the one-dimensional equivalent combustion zone, namely, $pA^{\epsilon/\epsilon-1}$ is assumed to be an appropriate approximation over the entire outer combustor wall. With these assumptions for the pressure distribution the integral equations can be solved to determine $\epsilon = \epsilon(P_s)$. However, with the additional boundary condition $dH/H = 0$ at the combustor exit, the value of ϵ, and therefore P_s, is uniquely determined.[1] With P_s and ϵ so

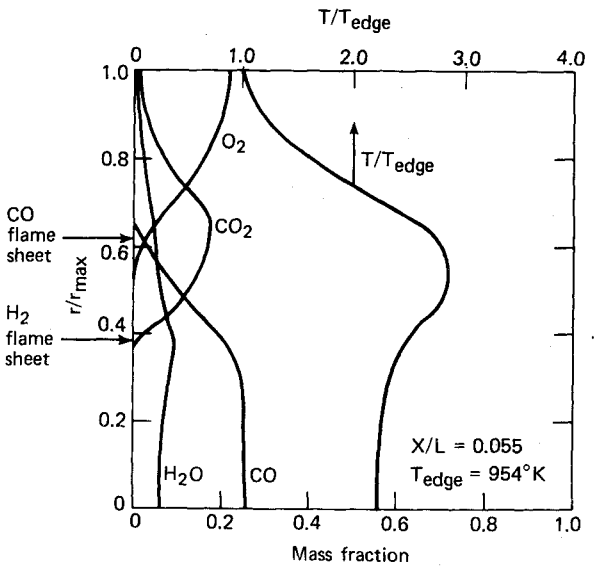

Fig. 10 Predicted profiles across the duct at Mach 7 with ER = 0.5.

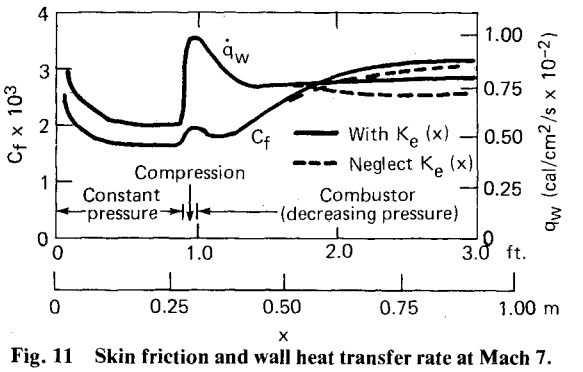

Fig. 11 Skin friction and wall heat transfer rate at Mach 7.

specified and the combustor shape $A(x)$ defined, then $P(x)$ is also defined. The combustor calculation uses this $P(x)$ and determines the shape of the boundary corresponding to $\Psi = \Psi_{max}$, which can then be compared with the physical duct area.

Ducted Jet Mixing and Burning Calculations

Using the information obtained as just described, the mixing and burning code was next run. The calculated shape of the boundary corresponding to $\Psi = \Psi_{max}$ for the given $P(x)$ distributions and the shape of the H_2 and CO flames for the two operating conditions are shown in Fig. 8. The CO flames are somewhat less than 1-m long, while the H_2 flames are only about 0.2-m long. Clearly, a 1.5-m combustion chamber is sufficient to provide for complete combustion for the selected cases with the diffusion controlled reaction assumption. The veracity of the modeling based on the incorporation of the results from the integral solutions to provide $P(x)$ is shown by the close correspondence of the boundary corresponding to Ψ_{max} and the actual combustor wall in the entire downstream portion of the flowfield. Indeed, at least the qualitative features of the separated zone on the outer boundary of the shock interaction region are also apparent.

The exit plane mass flux profile results shown in Fig. 9 indicate that even though combustion has been completed, residence time in the combustor is not adequate to yield uniform property profiles in the combustor exit plane. The degree of thrust decrement due to nonuniformity depends on the exhaust nozzle geometry.

Some detailed profiles across the duct at an axial station near the end of the H_2 flame are shown in Fig. 10 for the

Mach 7 case. The calculation was run with 30 radial points, and the full equilibrium computations were called for several points near the flames. At this station, the H_2 flame is at $r/r_{max} = 0.39$ and the CO flame is at $r/r_{max} = 0.61$. For all of the points with the full equilibrium calculations, the mass fractions of O, H, N, OH, and NO were negligible; however, O_2 was present inside and CO was present outside the CO flame. The flame sheet model could not predict that behavior.

Additional output from this calculation which is used as input for the wall boundary-layer calculations is the distribution of $u(x, \Psi_{max})$, $T(x, \Psi_{max})$, $Y_i(x, \Psi_{max})$, and $k(x, \Psi_{max})$. These correspond to $u_e(x)$, $T_e(x)$, $Y_{i,e}(x)$, and $k_e(x)$ for the boundary layer.

Combustor Wall Boundary Layer

Wall boundary-layer calculations for the Mach 7 case have been made. To obtain the initial conditions for the boundary layer at the front of the combustor, it was assumed that the outer surface of the inlet air duct could be represented by a constant-area tube 0.305-m long. To represent the pressure rise in the interaction shock region just ahead of the combustion zone, a linear variation from the conditions ahead of the precombustion shock over a length of 0.274 to 0.305 m was assumed. The remainder of the pressure distribution and the edge conditions were obtained from the mixing and burning analysis. The wall temperature was assumed constant at $T_w = 2000°R$.

Boundary-layer calculations were run to an axial distance of about halfway down the combustor. The variation of the skin friction coefficient based on local edge conditions C_{f_e} along the combustor wall is shown in Fig. 11. The region labeled *compression* ahead of the combustor shows the simplified representation of the interaction-shock region that was used. Calculations both with and without the influence of the higher k_e are shown. The C_{f_e} values are rather high for this high Reynolds number flow, and they do not decay roughly as $x^{-1/5}$ as would result for a constant-pressure flow. Thus, the indirect effects of the flame on the boundary layer are seen to be significant. The dimensional wall heat transfer rate also shown in Fig. 11 is more sensitive to the local pressure gradient. The qualitative response of C_f and $\dot{q}_w$ to the variations in edge properties can also be seen to be quite different. These heat transfer rates are rather large even though this case is lean overall and the flame does not impinge on the wall.

Discussion

A complete, modular calculation procedure for predicting the flowfield in the combustor of a scramjet with a center fuel jet has been developed. The various parts of the procedure have been tested against experimental data where available.

The results for the mixing and burning of the center fuel jet indicate that nonuniformity of the nozzle entrance profiles is likely to be a larger problem than attaining complete mixing for the type of model engine and the conditions studied. Both the wall heat transfer rates and the skin friction coefficients that can be expected in the combustor have been shown to be quite high. This has important consequences for design and performance predictions. The response of these two quantities to the local pressure gradient and to the rapidly varying boundary-layer edge conditions are rather different and not in phase. Lastly, the effect of impingement of turbulence from the jet mixing zone on the edge of the boundary layer is to increase the skin friction and heat transfer by about 10%.

Acknowledgment

This work was supported by the Naval Ordnance Systems Command.

References

[1] Billig, F. S., Waltrup, P. J., and Stockbridge, R. D., "The Integral-Rocket, Dual-Combustion Ramjet: A New Propulsion Concept," *4th International Symposium on Air Breathing Engines,* Lake Buena Vista, Orlando, Fla., April 1979, pp. 433-444.

[2] Schetz, J. A., Billig, F. S., and Favin, S., "Analysis of Mixing and Combustion in a Scramjet Combustor with a Co-Axial Fuel Jet," AIAA Paper 80-1256, June-July 1980.

[3] Schetz, J. A., "Turbulent Mixing of a Jet in a Co-Flowing Stream," *AIAA Journal*, Vol. 6, Oct. 1968, pp. 2008-2010.

[4] Schetz, J. A. and Favin, S., "Numerical Solution of the Near Wake of a Body with Propeller," *Journal of Hydronautics,* Vol. 11, Oct. 1977, pp. 136-141.

[5] Schetz, J. A., "A Simplified Model for the Combustion of Multicomponent Fuels in Air," *Combustion and Flame*, Vol. 15, Aug. 1970, pp. 57-60.

[6] Gordon, S. and McBride, B., "Computer Program for Calculation of Complex Equilibrium Compositions," NASA SP-273, 1971.

[7] Billig, F. S. and Dugger, G. L., "The Interaction of Shock Waves and Heat Addition in the Design of Supersonic Combustors," *Twelfth Symposium (International) on Combustion,* The Combustion Institute, Pittsburgh, Pa., 1969, pp. 1125-1134.

[8] Prandtl, L., "Über eine neues Formelsystem für die ausgebildete Turbulenz," *Nachrichten der Akademie Wissenschaften, Göttingen, Mathphys*, Van den Loeck & Ruprecht, Göttingen, 1945, pp. 6-19.

[9] Anderson, E. C. and Lewis, C. H., "Laminar or Turbulent Boundary-Layer Flows of Perfect Gases or Reacting Gas Mixtures in Chemical Equilibrium," NASA CR-1893, Oct. 1971.

[10] Fletcher, R. H., "On a Calculation Method for Compressible Turbulent Boundary Flows with Heat Transfer," AIAA Paper 71-165, 1971.

[11] Blottner, F. G., "Finite Difference Methods of Solution of the Boundary-Layer Equations," *AIAA Journal*, Vol. 8, Feb. 1970, pp. 193-205.

[12] Svehla, R. A. and McBride, B. J., "FORTRAN IV Computer Program for Calculation of Thermodynamic and Transport Properties of Complex Chemical Systems," NASA TN D-7056, Jan. 1973.

[13] Schetz, J. A., *Injection and Mixing in Turbulent Flow*, Vol. 68, *Progress in Astronautics and Aeronautics*—AIAA, New York, 1980.

[14] Zeiberg, S. L. and Bleich, G. D., "Finite Difference Calculation of Hypersonic Wakes," AIAA Paper 63-448, Aug. 1963.

[15] Chriss, D. E., "Experimental Study of Turbulent Mixing of Subsonic Axisymmetric Gas Streams," Arnold Engineering Development Center, AEDC-TR-68-133, Aug. 1968.

[16] Van Driest, E. R., "On Turbulent Flow Near a Wall," *Journal of the Aerospace Sciences*, Vol. 23, No. 11, 1956, pp. 1007-1011.

[17] Clauser, F., "The Turbulent Boundary Layer," *Advances in Applied Mechanics*, Vol. IV, Academic Press, 1956.

[18] Reichert, H., "Vollständige Darstellung der turbulenten Geschwindigkeitsverteilung in glatten Lutungen," *ZAMM*, Vol. 31, 1951, pp. 208-219.

[19] Coles, D., "Measurements of Turbulent Friction on a Smooth Flat Plate in Supersonic Flow," *Journal of the Aerospace Sciences*, Vol. 21, July 1954, pp. 433-448.

[20] Huffman, G. D., Zimmerman, D. R., and Bennett, W. A., "The Effect of Free-Stream Turbulence Level on Turbulent Boundary Layer Behavior," *Boundary Layer Effects in Turbomechanics*, AGARDograph No. 164, Dec. 1972.

[21] Waltrup, P. J. and Billig, F. S., "Prediction of Precombustion Wall Pressure Distributions in Scramjet Engines," *Journal of Spacecraft and Rockets*, Vol. 10, Sept. 1973, pp. 620-622.